Seasonal and diurnal variability of O_3, BC, and CO measured at the Rwanda Climate Observatory

H. Langley DeWitt[1], Jimmy Gasore[1,3,4], Maheswar Rupakheti[2], Katherine E. Potter[1], Ronald G. Prinn[1], Jean de Dieu Ndikubwimana[3], Julius Nkusi[3], and Bonfils Safari[4]

[1] Massachusetts Institute of Technology, Center for Global Change Science, Cambridge, MA, USA

[2]Institute for Advanced Sustainability Studies (IASS), Potsdam, Germany

[3]Ministry of Education, Climate Secretariat, Kigali, Rwanda

[4]Unviersity of Rwanda, Physics Department, Kigali, Rwanda

Abstract

Air pollution is understudied in sub-Saharan Africa, resulting in a gap in scientific understanding of emissions, atmospheric processes, and impacts of air pollutants in this region. The Rwanda Climate Observatory, a joint partnership between MIT and the government of Rwanda, has been measuring ambient concentrations of key long-lived greenhouse gases and short-lived climate-forcing pollutants CO_2, CO, CH_4, BC, and O_3 with state-of-the-art instruments on the summit of Mt. Mugogo (1.586° S, 29.566° E, 2590 m above sea level) since May 2015. Rwanda is a small, mountainous, and densely populated country in equatorial East Africa, currently undergoing rapid development but still at less than 20% urbanization. Black carbon concentrations during Rwanda's two dry seasons (DJF and JJA), which coincide with the two regional biomass burning seasons, are higher at Mt. Mugogo than in major European cities with daily (24 hour) during the dry season of around 5 μg m^{-3} (daily average range from less than 0.1 – over 17 μg m^{-3} for the entire measurement period). BC baseline concentrations during biomass burning seasons are loosely correlated with fire radiative power data for the region acquired with MODIS satellite instrument. The position and meteorology of Rwanda is such that the emissions transported from both the northern and southern African biomass burning seasons affect BC, CO, and O_3 concentrations in Rwanda. Spectral aerosol absorption measured with a dual-spot Aethalometer varies seasonally due to changes in types of fuel burned and direction of pollution transport to the site. Ozone concentrations peaked during Rwanda's dry seasons (daily measured maximum of 70 ppbv). Understanding and quantification of the percent contributions of regional and local (beyond large-scale biomass) emissions is essential to guide policy in the region. During the rainy seasons, local emitting activities (e.g., cooking, transportation, trash burning) remain steady, regional biomass burning is low, and transport distances are shorter as rainout of pollution occurs regularly. Thus local pollution at Mugogo can be estimated during this time period, and was found to account for up to 35% of annual average BC measured. Our measurements indicate that air pollution is a current and growing problem in equatorial East Africa.

1. Introduction

According to recent data collected and published by the World Bank, particulate air pollution in most African countries is above the annual average guideline values recommended by the World Health Organization (WHO). Despite this, little scientific research has been published on air quality in Africa, which can be approximated by the number of paper results from the search terms 'air pollution + country name.' World Bank collected data and model approximations estimate higher

52 $PM_{2.5}$ exposure in African versus European Countries (Figure 1). The WHO reported in
53 2013 that one in eight premature deaths globally can be linked currently to poor air
54 quality (WHO, 2013), while another, more recent report, showed that these deaths are
55 concentrated in developing countries (World Health Organization, 2016). Black
56 carbon (BC) is one of the major air pollutants emitted from Africa, mainly from
57 biomass burning as it is widespread on the continent during certain seasons. In
58 addition to affecting health, BC contributes to atmospheric heating and thus to climate
59 change (Ramanathan and Carmichael, 2008). Widespread crop fires in northern and
60 southern Africa, prevalent in boreal winter (December-January-February, DJF) and
61 austral winter and part of austral spring (June-July-August, JJA and September-
62 October), respectively, are known to increase aerosol and ozone concentrations in
63 this region and transported molecular and aerosol fire tracers associated with
64 elevated ozone have been measured as far as the Pacific and Indian Oceans (Field et
65 al., 2016; Real et al., 2010).
66 Rwanda is located in the middle of the two major seasonal biomass burning
67 regions of sub-Saharan Africa. Wide-scale biomass burning occurs to the north of
68 Rwanda during December-January-February (DJF) and to the south during June-July-
69 August (JJA). Rwanda's climate may exacerbate fire haze pollution effects, as Rwanda
70 experiences two dry seasons that occur at the same time as these two continental
71 burning seasons, making long range transport with low rainout efficiency likely.
72 Rwanda's prevalent wind direction also changes from northerly (DJF) to southerly
73 (JJA) at the same time as the large-scale biomass burning area shifts from north-
74 central Africa to southern Africa. Increase in incidence and amount of biomass

75 burning is thought to be one consequence of climate change in this region (Niang et
76 al., 2014). Southern Africa's biomass burning is also influenced significantly by human
77 activity, not just the climate (Archibald et al., 2010). Rwanda is positioned to
78 experience both large-scale (transported) haze due to fires and human activities and
79 local, diffuse emissions.

80 In addition to air quality issues, climate change (related to air pollution) may
81 also adversely affect Rwanda. The major pollutants from or ultimately increased by
82 biomass burning (particles, carbon monoxide, ozone) are also known short-lived
83 climate forcers. The main products exported (coffee and tea), the livelihood of the
84 majority of Rwandans (agriculture), and power (currently almost half of Rwanda's
85 power is hydroelectric) are all potentially affected by climate change. These issues
86 are similar across the region. Central Africa is expected to receive increased severe
87 rainstorms, which may lead to erosion and an uptick in vector-borne diseases (Niang
88 et al., 2014). Rwanda's mountainous topography and ubiquitous hillside agriculture
89 makes Rwanda venerable to floods and landslides. However, there is limited on-
90 ground data on air quality and climate change in Africa.

91 In order to advance our scientific understanding of air pollution, climate
92 change, and their impacts in Africa through generation of on-the-ground data, MIT
93 and the government of Rwanda have established the Rwanda Climate Observatory
94 (RCO). The RCO has a goal to measure long-lived greenhouse gases and short-lived
95 climate forcers/pollutants in East Africa. Since May 2015, CH_4, CO, CO_2, O_3, and BC
96 concentrations have been continuously measured, and N_2O measurements were
97 added in February 2017. The RCO is a part of the Advanced Global Atmospheric Gases

Experiment (AGAGE) network, a global network of high-frequency trace greenhouse gas measurements (Prinn et al., 2000), and is the first station of its kind in Africa. Rwanda was chosen as a location due to several factors. These factors include government interest from Rwanda and willingness to take on station maintenance, Rwanda's interest in growing its technical sector, readily available infrastructure in Rwanda to support the project, and a gap in climate data in this area of the world.

Here we present first results on diurnal and seasonal variations in short-lived climate forcers/pollutants related to air quality, focusing on O_3, CO, and BC observed at the RCO. This dataset is unique and unprecedented to the region. Information on the concentrations, sources, and time-dependent concentration variations of these air pollutants is essential in this rapidly changing area of the world. Data will not only advance our understanding of air pollution and climate change in the region but also potentially inform future policies on air pollution with sound science.

2. Experimental Methods: Rwanda Climate Observatory

2.1 Rwanda Climate Observatory Environment

The RCO is located in the Northern Province of Rwanda, near Byangabo on the summit of Mt. Mugogo (1.586° S, 29.566° E, and 2590 m above sea level). Mt. Mugogo is about 70 km (aerial distance) to the north-west from Kigali, the capitol of Rwanda (population of approximately 1 million), 20 km (south-west) from the next major city, Musanze (population of around 100,000), and 60 km north-east from the Lake Kivu region (Gisenyi, Rwanda and Goma, DRC, combined population of approximately 1 million). A dirt road reaches the base of the mountain, about 500 m below the summit

where the RCO is located, and a diesel generator is installed on the road at the base. Inlets were installed on both the roof of the Observatory (10 m above ground level) for O_3 and BC) and on a Rwanda Broadcasting Authority Tower (35 m above ground level) for CO, CO_2 and CH_4. There is a small Rwandan army camp adjacent to the measurement site and a eucalyptus forest and a mix of agricultural fields and scattered rural houses surround the immediate vicinity of the RCO (Figure 2).

The high altitude and remote positioning of Mt. Mugogo allows sampling of regional air masses from throughout East Africa depending on prevailing meteorological conditions, as well as local pollution (as the dense population but low urbanization of Rwanda means that direct human influence is ubiquitous except within the national parks). Kigali and the Lake Kivu region are approximately 1000 m in altitude below the station height and their altitude (~1500 m) can be used as the base of local pollution. The majority of air masses transported to Mugogo originate below 5 km above ground level. Approximately 20% of yearly air masses measured at Mugogo's summit originate from 0-1 km above ground level (certainly within the polluted boundary layer), and approximately 36% below 2 km (potentially within the polluted boundary layer) (from HYSPLIT analysis). During mid-day, Mugogo's summit is likely within the regional polluted boundary layer, but during the later evening it is likely above. Complicating this issue is the network of farms and houses along the mountainside near Mt. Mugogo.

2.2 Instrumentation and Calibration

143 Details on the instruments sampling at the RCO are compiled in Table 1. $PM_{2.5}$
144 BC (particulate matter $_{2.5}$ micrometers in diameter or less) was measured using a
145 Magee Scientific 7-wavelength Aethalometer with dual-spot technology that is able to
146 correct for filter loading artifacts (Drinovec et al., 2015). A cyclone $PM_{2.5}$ impactor was
147 installed on the inlet to remove larger particles and covered with an insect net. Air
148 was passed through a filter once per day to collect blank data and examined to ensure
149 the instrument baseline was correct. If high, the filter was changed and the blank
150 rerun. Flow was calibrated once per year and after major instrument movement and
151 changes, while the optical performance was calibrated with a neutral density filter kit
152 once per year. Data was recorded every minute at a 5 liter per minute (LPM) flow
153 rate and particles were captured on a quartz fiber filter tape. The air stream was not
154 dried and the relatively humidity (RH) was not controlled, which could lead to
155 increased uncertainty during periods of high relative humidity. RH recorded at the
156 station varied by approximately 5% over the day and from 60-85% monthly,
157 depending on the season. The 880 nm channel was used to calculate the concentration
158 of BC but all channels were examined to determine reasonable data (comparing to
159 literature values). Five minute data (not pictured) was used to detect very local
160 pollution and remove influence of short-lived local fires and BC from the generator
161 500 m below the station. Spikes in BC concentrations that lasted for less than 15
162 minute with values higher than 25,000 ng m^{-3} were removed, along with
163 corresponding CO.
164 CO mixing ratios were measured in real-time using a cavity ring-down
165 spectrometer (G2401, Picarro, USA). Sampled, laboratory, and calibration air were

dried with a Nafion drier inside an Earth Networks calibration box to increase the accuracy of the Picarro water vapor correction (Welp et al., 2013). Three NOAA-standard calibration tanks were used for calibration spanning normal ambient concentrations and calibrations were performed once per day initially to check for linearity of instrument's response (Gasore and Physics, 2018). An O_3 monitor (T400, Teledyne Advanced Pollution Instrument, USA) was used to measure O_3. Regular checks were performed using internal span and zero O_3 calibrations, and non-passing data was removed. Flow was calibrated two to three times per year.

Meteorological data (ambient temperature, relative humidity, pressure, wind speed, wind direction and rainfall) were collected with an automatic weather station (WXT520, Vaisala, Finland). The weather station was attached to a fixed, hinged arm 35 m above ground level and connected to the communications tower, level with the $CO/CO_2/CH_4$ inlet, with a 2 m clearance from the tower. The weather station was calibrated when delivered and recalibrated during repairs (once during the two year measurement period).

In addition to the described instrument checks and data quality control procedures, station technicians visited the station once daily (except Sundays) and performed visual checks of all instruments except the meteorological station, which was examined once per quarter manually by climbing the tower. They also notified the station chief scientist immediately of any issues (instrument warnings, generator issues, data coverage outages) and worked to address these issues.

3. Results and Discussion

3.1 Seasonal Variation in BC, CO, and O_3

189 Figure 3 shows a summary of the data, including daily and 15 minute averaged
190 BC, O_3, and CO data and meteorological data. Daily averages were examined to probe
191 overall increases in regional pollutants, while 15 minute averages were used to detect
192 local pollution.
193 Rwanda has two rainy seasons roughly occurring in March-April-May (MAM)
194 and September-October-November (SON), and two dry seasons during December-
195 January-February (DJF) and June-July-August (JJA). This generalized definition and
196 durations of the seasons are used the purpose of comparing data for multiple years
197 and is used throughout this paper. High variations in BC concentrations can be seen in
198 the BC time series (Figure 3) ranging from below 100 to above 20,000 ng m^{-3}, with an
199 average value of 1,700 ng m^{-3} (standard deviation: 1,600 ng m^{-3}). Peak concentrations
200 corresponded to dry seasons. CO and O_3 mixing ratios also increased during the dry
201 seasons compared to the rainy seasons, though not as pronounced as the BC
202 increases. This decrease is partially due to the efficient rainout of black carbon
203 particles during the rainy season. The diurnal, weekly, and monthly variations in
204 concentrations of each species, normalized to their average, are shown in Figure 4.
205 It has been known for some time that wide-scale biomass burning in sub-
206 Saharan Africa has a large seasonal effect on the atmosphere (e.g., Archibald et al.,
207 2010; Crutzen and Andreae, 1990). Understanding and separating these seasonal
208 effects from anthropogenic emissions can be difficult without continuous data sets
209 both during and outside of this period, especially as both biomass burning and
210 anthropogenic emissions in this region of the world emit BC, CO, and PM. Biomass

burning emissions have also been shown to affect O_3 formation under the right meteorological conditions.

To explore the sources of BC and CO, at the RCO, seven-day HYSPLIT back trajectories were run every 6 hours using NCEP/NCAR reanalysis meteorological data (2.5 x 2.5 degree resolution) (Kalnay et al., 1996). This analysis provided insights on the approximate origin and trajectories of air masses before arriving at RCO measured at the RCO. These HYSPLIT back trajectories were separated into DJF, MAM, JJA, and SON and are shown with MODIS satellite fire count data colored by fire radiative power (FRP, W m^{-2}) (Figure 5). The MODIS fire count data and radiative power are used strictly for qualitative, not quantitative, purposes in this work. Here we observe that, as major biomass burning sites moved to the north and west in DJF, transport direction was also primarily northerly, and as biomass burning move to Southern Africa in JJA, the prevailing wind directions were also southerly. Although Rwanda itself had few large-scale fires, its geographical position and meteorology meant that it experienced transported fire haze from both major burn seasons. Black carbon measured at the station tracked fairly well with summed daily FRP for sub-Saharan Africa (Figure 5). This suggests that transport from regional biomass burning has a twice-yearly effect on BC concentrations in Rwanda, despite the different locations of the biomass burning in sub-Saharan Africa.

To further examine pollution transport to the RCO, the HYSPLIT back trajectory geographical areas were gridded (using the R Openair package, (Carslaw and Ropkins, 2012)) and merged, using date and time, with measured BC concentrations and mixing ratios of CO. This was done to generate concentration-

234 weighted back trajectories (cwt) for each season (more details on cwt available in
235 (Hsu et al., 2003; Seibert et al., 1994))(Figure 6). Trajectory time in each grid and
236 arrival time of each air mass were taken into account in this model to predict the
237 likely source regions and emission concentrations of pollutants measured at the RCO.
238 This was done to determine likely source regions of air pollution at the RCO by
239 comparing arrival times of air masses to the RCO and the time series of pollutants.
240 This method has proven fairly effective at identifying emission sources when
241 comparing predicted emission regions to emissions inventories (Lupu and Maenhaut,
242 2002) and is good as a rough estimate of emission regions with no apriori
243 information (Kabashnikov et al., 2011).
244 BC and CO appeared to originate from similar areas, as expected due to their
245 overlapping sources of inefficient combustion and biomass burning. During JJA,
246 significant BC and CO appeared to originate from southern Africa and Madagascar, as
247 well as from local sources near the RCO. During DJF, the source of these pollutants
248 appeared to be much closer to the RCO, as major fires in the DRC and Uganda were
249 also closer to the station. Throughout the measurement period, but particularly DJF,
250 the Lake Kivu region also appeared to be a source of BC and CO. The Lake Kivu region
251 is densely populated and use of both cook stoves and diesel generators is common.
252 In addition to direct emissions of BC and CO, other emissions such as volatile
253 organic compounds and oxides of nitrogen from biomass burning are known to affect
254 tropospheric O_3 concentrations (Jaffe and Wigder, 2012; Sauvage et al., 2005). It
255 appears that such emissions could have played a role in the observed seasonal
256 increase in O_3 mixing ratios of approximately 20 ppb in DJF and 25 ppb in JJA above

rainy season levels at the RCO. This increase of about 5 ppb O_3 during JJA versus DJF was potentially due to the mixing of biomass burning emissions with anthropogenic emissions from east African cities such as Nairobi, Dar Es Salam, and Kampala during the JJA dry season. It also could have been the result of generally higher solar radiation during the JJA season in Rwanda (Safari and Gasore, 2009). A mix of biomass burning and anthropogenic emissions from southern Africa could have been transported to Rwanda after photochemical aging and processing. Direct source apportionment of O_3 is difficult as O_3 is formed from the right combination of VOCs, NOx, and favorable meteorological conditions (Baier et al., 2015; Geddes et al., 2009; Gong et al., 2017; Monks et al., 2015). During the DJF dry season, fires are closer to Rwanda and away from major urban areas. During June and July, a loose correlation (R=0.47 and 0.45, respectively) between O_3 mixing ratios and BC concentrations was observed, while no correlations (R=-0.04, -0.15, and 0.07) were observed in December, January, and February.

3.2 Absorption Angstrom Exponent and BC Source Apportionment

It is important to understand the pollution emission sources in East Africa, beyond large-scale biomass burning, in order to enact policies and actions to reduce these emissions. One way scientists have estimated fuel combustion versus biomass burning BC particulate is by measuring the color of the particles (wood smoke particles have enhanced absorption in the UV, while fossil fuel combustion particles have flat absorption over all wavelengths)(Kirchstetter and Thatcher, 2012; Sandradewi et al., 2008). The Aethalometer's seven wavelengths allow measurement of the wavelength-dependent aerosol absorption and the calculation of absorption

coefficients that can be used to infer the potential sources of BC aerosol (Drinovec et al., 2015; Sandradewi et al., 2008) measured. Theoretically, from the wavelength dependence of aerosol absorption, BC from fossil fuel and wood smoke can be differentiated (Sandradewi et al., 2008). Though this two-component model can provide a valuable knowledge on knowledge on source attribution of BC this model has some limitations. This model is more accurate if calibrated to local conditions as burning and aging during transport affects aerosol 's wavelength-dependent absorption (Dumka et al., 2013; Harrison et al., 2012), as different fuels and wood biomass burning creates aerosol with different radiative properties and the standard model, based on European studies, has been shown to be less applicable in developing countries (Garg et al., 2016).

From the Aethalometer data, wavelength dependence of absorption coefficients and the absorption Ångstrom exponent (AAE) were calculated and compared to literature values of biomass burning and fossil fuel combustion (Figure 7). The AAE is a dimensionless property commonly used to characterize the wavelength-dependent absorption of BC and gives clues on the source and/or aging of BC when compared to laboratory and other ambient studies (Chung et al., 2012; Lack and Langridge, 2013; Russell et al., 2010; Yuan et al., 2016). The AAE values assigned for the standard Aethalometer model separating the BC from biomass burning and fossil fuel combustion are two and one, respectively (where two represents an average AAE for woodsmoke of different types and ages) (Kirchstetter et al, 2004; Sandradewi et al, 2012; Drinovec et al. 2015). In this work, standard mass absorption cross-sections (MACs) for each wavelength provided by the manufacturer of the

Aethalometer were used to calculate the absorption coefficient (b_{abs}) at each wavelength. For pure BC from fossil fuel, $b_{abs} \sim 1/\lambda$ and the AAE between two wavelengths (470 nm and 950 nm) is 1 using the equation $\ln(b_{abs}\lambda_1/b_{abs}\lambda_2)/\ln(\lambda_2/\lambda_1)$.

The average AAE (averaged for entire measurement period between July 2015 and January 2017) was calculated to be 1.65 (+/- 0.14) at the RCO using the 470 and 950 wavelength absorption and MACs (Figure 10)(Sandradewi et al., 2008; Drinovec et al. 2015). These wavelengths were chosen as the AAE calculated from 470 and 950 is generally comparable with other literature values(Saarikoski et al., 2012). The calculated AAE values were on par with AAE calculated from measurements taken in areas heavily influenced by biomass burning (Chung et al., 2012; Lack and Langridge, 2013; Russell et al., 2010; Saleh et al., 2013; Sandradewi et al., 2008; Yuan et al., 2016). Past studies have reported an AAE of 1.2-$_{2.5}$ for biomass burning aerosol (Andreae and Gelencsér, 2006; Chung et al., 2012; Russell et al., 2010; Saleh et al., 2013, 2014). While daily only small variations (+/- 0.05) for AAE were observed (, significant seasonal differences in this value were found, with monthly averaged values ranging from 1.5 (dry season) to 1.9 (at the end of the long rainy season). This seasonal difference is shown with the 30 day running mean of the AAE (Figure 7). Studies in southern Africa measuring savanna and crop burning found an AAE of around 1.45 for ambient black carbon aerosol, and in the dry season savanna and crop burning are the prevalent type of large-scale biomass burning in sub-Saharan Africa (Russell et al., 2010). The AAE calculated from the Aethalometer data at the RCO was higher during the rainy season when local emissions dominated our measurements (Figure 7). Eucalyptus burning, the most prevalent burning near the station (for

charcoal making, cooking fires, brick kiln fuel) was measured in laboratory experiments to have a higher AAE than savanna burning (AAE of 1.71 +/- 0.50 calculated between 405 and 781 nm wavelengths)(Chung et al., 2012). Eucalyptus trees and savanna burning were certainly not the only two types of solid biofuel influencing measurements at the station, but the difference in AAE of aerosols produced from different fuels means that the AAE will have large variations based on fuel wood or other biomass used and this was reflected in our data.

Using the Aethalometer model with standard inputs not accounting for the different types of fuel used in East Africa versus Europe, a high influence of fossil fuel black carbon emissions was calculated: in the dry season, over 50% of black carbon was assigned to be fossil fuel in origin (Figure 7). Fossil fuel emissions certainly influenced the pollution at the RCO, as air masses from Kigali, Kampala, Nairobi, and Dar es Salaam were transported to the station. These cities have high black carbon emissions from generators, fossil fuel power stations, and older diesel vehicles but would also have significant biomass cook stove emissions (Gatari and Boman, 2003; Koch et al., 2009; Mkoma et al., 2009; van Vliet and Kinney, 2007). However, at <10% fuel demand of fossil fuel (all types, see Table 2) versus >90% wood and charcoal fuel demand, even if the g BC per kg fuel from diesel was 4x higher, and all fossil fuel use was unregulated diesel (unlikely), well under half of the measured BC should be from fossil fuel combustion emissions. Aging with transport would increase the AAE of the aerosol, not decrease, so aging should not cause this seasonal difference as transport distances of BC are longer during the dry seasons.

In order to gain more insights into the sources of BC we also examined the BC:CO. CO is also released by inefficient combustion and the ΔBC: ΔCO ratio can be different for different emission sources. In order to calculate this ratio we first converted the CO mixing ratios to concentrations (in $\mu g\ m^{-3}$), and then subtracted the 95^{th} percentile values for CO and BC from their respective concentrations. For the entire data set, the ΔBC: ΔCO (both in $\mu g\ m^{-3}$) ratio was 0.014 (R^2 0.79, n = 40523). The ΔBC: ΔCO ratio varied seasonally, with monthly average peaks reaching 0.016 in December, February, and July and lows below 0.01 in April. The average ratio of 0.014 for the measurement period was almost twice as high as in biomass burning plumes sampled over West Africa in an aircraft campaign (0.0072) (Moosmüller and Chakrabarty, 2011) but on par with or lower than measurements taken during the INDOEX campaign in the Indian Ocean (Dickerson et al., 2002). A study in Germany and Mexico found a correlation between diesel vehicle use and higher BC:CO (Baumgardner et al., 2002), while other studies have also found an increased ΔBC: ΔCO during periods more influenced by biomass burning (Pan et al., 2011). A study in India found no correlation in biomass-burning and fossil fuel-influenced ΔBC:ΔCO air masses (Sahu et al., 2012), as there are a wide range of ratios measured from the same source (Dickerson et al., 2002; Sahu et al., 2012). The high ΔBC:ΔCO ratio at the RCO could be due to the prevalence of older diesel engines in the country, which emit more BC to CO than newer engines (Cai et al., 2013), but, as the highest value occurs during the Rwanda dry seasons and the continental biomass burning seasons , likely the ratio is governed in part by rainout as BC is more easily removed by wet deposition than CO. In this study, we were not able to use this ratio to further

separate biomass burning BC from fossil fuel combustion BC. However, this inconclusiveness highlights the need for further study, as ascribing a source to local pollution is important. Further work on emissions profiles relevant to sub-Saharan Africa could clarify these issues. Cookstoves, cookfires, agricultural and trash burning, and older diesel combustion emissions are all likely sources of BC and could be targeted by government policy. Understanding the most important source of local pollution is important for developing efficient government policies for air quality.

3.3 Examination of Local and Regional Pollution

The continuous collection of BC, CO and O_3 data during the dry and rainy seasons allowed examination of both transported and local pollution. Here we define local pollution as pollution originating within twelve hours transport time under typical wind speed conditions (<150 km, including both Rwanda and the border areas with DRC and Uganda). During Rwanda's rainy seasons, the continental fire count is also at a minimum, reducing large-scale biomass burning influence. The region's emissions are from small-scale agricultural burning, charcoal making, cooking fires, brick production (located in the valley below the station and throughout the region), vehicles, diesel and heavy fuel-oil power plants, and diesel generators. These activities continued throughout the rainy season and dry season at similar rates.

The baseline daily average BC concentration in the rainy season remained at 0.5-1 $\mu g\ m^{-3}$ after 12 hour periods without rain, which could be considered as contributions of small but numerous diffuse emission sources to daily BC concentration in this region. These values, while significantly below those during the biomass burning affected seasons, are not negligible. If all BC during the rainy seasons

394 is assumed to be local in origin (within one day of transport, as typically rain occurs
395 each day during the rainy season), and this level remained the same throughout the
396 year, yearly average contribution of local emissions to BC would vary between 18-
397 100% of the total measured BC concentration at the RCO. The shoulder months of
398 September and February have been removed from this calculation as they have both
399 rain and biomass burning influence, but on a yearly scale, around 35% of BC
400 concentration measured at the station could originate from local emissions. This
401 estimate is a high estimate as transport of BC is still possible above the boundary
402 layer, but it is on par with previous estimates of the contribution of savanna and
403 forest burning BC emissions versus other emission sources in sub-Saharan Africa
404 (Bond et al., 2013).

405 **3.3.1 Diurnal Variations in BC, CO and O_3**

406 Diurnal variations in concentration of pollutants can provide important
407 insights into information on local as well as regional pollution emission sources.
408 Boundary layer height and whether or not the station is measuring the free
409 troposphere or the polluted boundary layer is also important for understanding
410 diurnal changes in pollutant concentrations (Nyeki et al., 1998). Diurnal variations in
411 BC concentrations, CO mixing ratios and O_3 mixing ratios observed at RCO in different
412 seasons are shown in Figure 8. At the RCO, the O_3 mixing ratio exhibited a diurnal
413 cycle with a peak in concentration in the evenings (after ~ 8 pm), with steady levels
414 through the night and a minimum during mid-day. The increase of O_3 in the later
415 evening is likely mainly regional O_3 transported above the boundary layer measured
416 at night (as the boundary layer height lowered), but some regionally formed O_3 could

417 also be transported to the station by the evening. Similar diurnal O_3 profiles were
418 found at other mountain locations remote from urban centers (Zhang et al., 2015).
419 This diurnal pattern persists in all seasons (Figure 8) and occurred on daily time
420 scales. The differences in diurnal minima and maxima were highest in the June-
421 August period, and lowest in the December-February period. This difference may be
422 due to the differences in biomass burning proximity (far in JJA, closer in DJF), primary
423 wind direction (southerly versus northerly), and also solar intensity (highest in JJA,
424 (Safari and Gasore, 2009)).

425 BC had mid-morning and early evening (~ 6 pm) peaks that coincided with
426 both cooking times and kerosene/generator use times (sunset at 6 pm each night),
427 indicating local influence on BC, before the station was outside of the boundary layer
428 in the evening. These peaks occurred approximately two hours before the O_3 peak
429 each evening, further indicating some regional or local influence. Regional transport
430 of BC higher in the atmosphere should be greater in JJA/DJF (more BC) and solely
431 boundary-layer driven BC concentration changes would be greater during these
432 times, but the normalized diurnal changes from daily baseline to daily peak remain
433 similar throughout the seasons. Additionally, no persistently higher nighttime (after 8
434 pm) BC baseline levels were observed in these data. CO mixing ratios had a similar but
435 less pronounced diurnal variation.

436 **3.3.2 Case Study: High and Low Periods of Black Carbon**

437 Seasonal variations are too long to fully capture local pollution events. To
438 further examine local pollution in 2016, high BC time periods during DJF (2/12-2/16)
439 and JJA period (8/3-8/6), and one period of low black carbon in the MAM period

(5/18-5/22) were examined for their BC:CO ratio and correlation, relationship of O_3 to CO, and AAE (Figure 9). From this figure, no clear trends are observed. The BC:CO is 10 with an R^2 of 0.48 for the polluted DJF period, 8 with an R^2 of 0.47 for non-polluted period in May, and 16.6 with an R^2 of 0.72 for the polluted JJA period. The average AAE for the May period was 1.79, for February 1.53, and for August 1.53 as well. Unfortunately, no O_3 data was available for the August period. O_3 in February was loosely correlated with CO (R^2 0.17) and averaged 39 ppbv, with a peak value of 43. O_3 in May had averaged 26 ppbv with a peak of 34 ppbv, and no correlation with CO.

During the May period, spikes in very local pollution can be seen (Figure 10). These hour plus increases in BC happen at regular cooking times in the valley and, due to their shorter (hourly) time scales of rise and fall, cannot be explained by changes in boundary layer conditions. The diurnal patterns of increased BC during cooking times persist during the polluted period, but on a baseline of regional pollution. Some of the diurnal variability in black carbon background can be attributed to boundary layer conditions, seen with the slow and steady changes over the course of the day not confined to the timescales of activity in the valley.

3.3.3 Potential Twice-Yearly Influence Biomass Burning in equatorial Africa

The BC in Rwanda has peaks in both dry seasons, and these peaks correlate well in time with the FRP in sub-Saharan Africa, as shown in Figure 5. However, the site in Rwanda is one site, and drawing a conclusion on regional seasonal pollution trends is difficult without other data. BC is only one component of $PM_{2.5}$. Other components of $PM_{2.5}$ include dust, organic carbon, nitrates, sulfates, and ammonium.

462 BC is indicative of combustion, and when BC rises due to combustion processes, often
463 $PM_{2.5}$ will rise (though combustion aerosol contains a significant organic fraction).
464 Although no continuous measurements of BC are widely reported in sub-
465 Saharan Africa, recently the US Embassies in Addis Ababa, Ethiopia, and Kampala,
466 Uganda have begun continuously measuring $PM_{2.5}$ concentrations. The raw data is
467 collected and reported online on the OpenAQ platform (OpenAQ.org). This dataset on
468 $PM_{2.5}$ concentrations in major cities over different seasons in this region has been
469 valuable in gaining basic insights into the seasonal characteristics of $PM_{2.5}$
470 concentrations in the region (Figure 11). While $PM_{2.5}$ is not the same as BC, biomass
471 burning is thought to be a major contributor to $PM_{2.5}$ in sub-Saharan Africa. By
472 examining the $PM_{2.5}$ concentration in a city in the same region as Rwanda (equatorial
473 east Africa) and a different region (further north), increased understanding on the
474 impact of the dual biomass burning seasons for different regions in sub-Saharan
475 Africa's air quality can be understood.
476 The $PM_{2.5}$ concentrations in both Addis Ababa and Kampala showed clear
477 seasonal patterns, though the seasonal patterns differed at the two sites. Addis Ababa
478 (Ethiopia) is much further north than Rwanda and Ethiopia is in general higher in
479 elevation than Rwanda (though at 2355 m, not higher than the RCO) and closer to the
480 Indian Ocean. In Addis Ababa, the dry season is also in DJF, but measured $PM_{2.5}$
481 concentrations were low during this season. HYSPLIT back trajectory calculations
482 confirmed that air masses during this time of the year originated over the ocean, not
483 from the continent. Kampala, Uganda is close to Rwanda, near the equator, and has
484 similar seasonality. Rainy and dry season extrema are shown in the available

485 Kampala $PM_{2.5}$ data, with an enhancement during February and JJA of around 15 to
486 25-30 μg m^{-3}, respectively, above $PM_{2.5}$ concentrations during other months.
487 While not pictured here, South Africa has the most air quality monitoring stations of
488 any sub-Saharan African country. Results from these stations show a $PM_{2.5}$ peak in
489 the southern burning season (June-October), though June-July was mostly due to local
490 heating (Hersey et al., 2015) and August-October was related to biomass burning
491 (Horowitz et al., 2017; Tesfaye et al., 2011).

492 From these data, it appears that African countries near the equator may be
493 positioned to experience six months per year of transported regional fire haze, from
494 both the northern and southern biomass burning seasons. This is potentially unique
495 to the region and this effect may be seen in other pollutants and short lived climate
496 forcers. In fact, beyond BC and $PM_{2.5}$, the MOZAIC campaign in the late 1990s and
497 early 2000s measured ambient O_3 mixing ratios at the Nairobi, Kampala, and Kigali
498 airports. This campaign found Kigali, despite its smaller size and lower vehicle count,
499 to have the highest O_3 mixing ratios among them (Sauvage et al., 2005). They
500 measured a similar in magnitude increase in surface O_3 mixing ratios during the JJA
501 season in Rwanda as our measurements at the RCO, although DJF was not measured
502 in their work.

503 O_3 measurements were made in Brazzaville, Republic of the Congo during
504 January and February O_3. While much further west than Rwanda, in Brazzaville O_3
505 mixing ratios also increased during January and February, parallel to Rwanda, with
506 monthly averages during January and February 25 ppb greater than the minimum of
507 <30 ppb in April (Sauvage et al., 2005). This suggests influence from northern

hemisphere biomass burning to O_3 mixing ratios at Brazzaville. O_3 in JJA at Brazzaville was almost 30 ppb higher than in January and February, however, so transport of air mass from the south and southern Africa biomass burning had a greater influence on O_3 in the region than transport from the north and biomass burning in central Africa. The 1992 SAFARI campaign also measured O_3 in sub-Saharan Africa throughout all seasons, and measured a seasonal ozone concentration peak during the JJA period for central and southern Africa (Thompson et al., 1996). A separate, large peak for DJF was not as observable in the SAFARI data (Thompson et al., 1996). SAFARI measurements took place prior to 1993, meaning that significant development in sub-Saharan Africa could have taken place between the SAFARI campaign and the MOZAIC campaign (1997-2003) that could drive the increasing O_3 in DJF as well as JJA over a period of almost a decade. More recent measurements were made in a 2000 SAFARI campaign, but not as far north as the previous SAFARI campaign (Otter et al., 2002) and the positioning of the measurements could have also had an effect on O_3 seasonality, as southern Africa is more influenced by biomass burning from August-October. The SAFARI campaign measured the total column O_3, not the ground-level O_3 mixing ratios, so data are not directly comparable.

4. Conclusions

In this work, we present the first long-term and continuous measurements of short-lived climate forcers for a nearly two-year period from July 2015 to January 2017 at the Rwanda Climate Observatory located at Mt. Mugogo in Rwanda. From these observations, we find that:

1. During Rwanda's two dry seasons, transported pollution led to high black carbon and carbon monoxide levels at the RCO, surpassing concentrations measured in many major cities elsewhere. Emissions from large-scale crop and savanna fires could have a wide-reaching effect on this region and likely drive the increased BC and O_3 measured during DJF and JJA by our study and O_3 by past studies in equatorial Africa. The dense population of equatorial East Africa and the double impact of the two fires seasons could lead to significant public health problems for the population in Rwanda and equatorial East Africa as exposure to elevated levels of $PM_{2.5}$ and BC concentrations occurs six months out of the year.
2. Local emissions beyond large-scale biomass burning influence were constant and estimated to contribute up to 35% of the annual average measured black carbon concentration, if black carbon during the rainy season was assumed to be completely local (Rwanda and neighboring countries) in origin (ranging from 0.5-1 $\mu g\ m^{-3}$ daily average measured BC). These local emissions, from different combustion sources (e.g., cooking fires, inefficient diesel generators and engines with sub-standard fuel use, solid biomass fuel burning, small agricultural fires), are likely concentrated in the densely populated Rwanda and Lake Kivu economic area. Rwanda's population is growing quickly. As these local emissions are related to

population density, air pollution will likely increase unless there is government intervention.

3. Different combustion fuel and burning practices in Europe and East Africa calls into question the accuracy and applicability of a two-component model for estimating BC from fossil fuel combustion and biomass burning using AAE approximations for biomass burning and fossil fuel combustion aerosol measured in Europe for use in East Africa. There may also be different mass absorption cross-sections for aerosols measured at the RCO than in Europe or North America. This shows the need for multiple on-ground measurements to fully understand pollution sources in different regions of the world, notably in Africa. However, seasonal variations in the wavelength dependence of ambient BC particles did point to different sources of BC particles and this should be further explored in future studies.

4. The measurements we have provided in this study will be useful in advancing atmospheric science in Rwanda, which has limited long-term and in-situ atmospheric data.

These data and analyses, while acknowledging the high influence of regional biomass burning, also show that measurable decreases in air pollution could be achieved within eastern and central Africa with targeted local policies, emphasizing cleaner diesel vehicles and generators, reduced wood-fuel reliance for cook stoves, and improved cook stoves to burn biomass fuel more efficiently. Currently, over 2

million households in Rwanda rely on wood burning (including charcoal) for cooking. While reducing this number will have significant economic costs, putting in place infrastructure for alternative cooking fuels (pellet stoves, LPG stoves, electrical stoves) could help the country avoid even higher local air pollution emissions and associated adverse impacts as the population grows. Diesel-fueled minibuses, common transport between towns in Rwanda and within Kigali, and older diesel vehicles are also high emitters of black carbon but newer vehicles with emissions control technology may be economically beyond the reach of local bus companies and citizens. Continuing to grow electrical capacity and connection will reduce the use of kerosene lanterns and diesel generators, and will reduce air pollution if additional energy capacity is achieved through renewable sources (solar, hydropower). The huge influence of regional biomass burning, exacerbated by equatorial East Africa's meteorology, and the potential influence of anthropogenic emissions from major cities on O_3 formation in these regions must also be examined as this area develops. Halting slash-and-burn agriculture, reducing trash incineration, and developing ways to warn the population during periods of high pollution from naturally occurring savanna and forest fires should be an important agenda for regional discussions on environmental, public health, and other development issues.

6. Future Work

The government of Rwanda is working to establish an air quality and climate change monitoring network throughout the country to measure ambient criteria air pollutants and other key climate change related components of atmospheric pollution. Building knowledge of air quality and climate change related emissions in this data-

poor area of the world is essential to fill the large data and knowledge gap in this region. Adding ground-based measurements, comparing measurements to satellite data, using data to evaluate and improve existing emission inventories, improving accuracy of global/regional air quality and climate change models, and using data for quantification of impacts of air pollution and climate change will help local governments design appropriate mitigation strategies rooted in data and local context.

7. Data Availability

This data will be made available at the AGAGE website, https://agage.mit.edu/data/agage-data. All data used in this article will be made available as of publication and data from this project on a rolling basis after quality control.

Acknowledgments:

We thank the generous MIT alumni donors to the MIT-Rwanda Climate Observatory Project that provided the funds to purchase, develop and install most of the instruments at the Rwanda Climate Observatory. Additional funds for this purpose were provided by the MIT Center for Global Change Science. COMESA provided the funds to purchase and install the Aethalometer at the RCO. We also thank the Government of Rwanda and the Rwanda Ministry of Education, specifically Mike Hughes, Vianney Rugamba, and Dr. Marie Christine Gasingirwa, for supporting this project, including funding the staffing and infrastructure costs of the Rwanda Climate Observatory and the University of Rwanda for providing laboratory space and infrastructure for instrument testing. We thank Dr. Arnico Panday who provided

guidance during the initial stages of this project. We also wish to acknowledge the essential contributions of the Mugogo station technical experts Theobard Habineza, Modeste Mugabo, Olivier Shyaka, and Gaston Munyampundu, and RBA technician Yves Fidele, without which running this station would be impossible.

627 Table 1: Instruments used in this study and measurement period used for analysis

INSTRUMENT	SPECIES MEASURED	MEASUREMENT PERIOD	AVERAGE VALUE	MIN VALUE	MAX VALUE
PICARRO G2401 CAVITY RING DOWN SPECTROMETER	CO_2, CO, CH_4, H_2O	MAY 2015-JANUARY 2017	215 (CO ppbv)	63(CO ppbv)	663(CO ppbv)
MAGEE SCIENTIFIC AE33 7-WAVELENGTH AETHALOMETER	BLACK CARBON ($PM_{2.5}$, CYCLONE IMPACTOR ON INLET)	MAY 2015-JANUARY 2017	1692 (ng m^{-3})	8 (ng m^{-3})	17445 (ng m^{-3})
TELEDYNE T400 API	O_3	MAY 2015-JANUARY 2017	40 (ppbv)	10 (ppbv)	84 (ppbv)
VAISALA WXT	MET PARAMETERS (RH, WS, WD, T, P)	JULY 2015-JANUARY 2017			

Table 2:

Fuel Demand in Rwanda (2016, Rwanda Ministry of Infrastructure)

Fuel Type	Demand
Petrol	120442 kL
Diesel	178529 kL
Kerosene	22288 kL
Heavy Fuel Oils	59292 kL
Jet-A	18235 kL
Wood (charcoal + natural)	4,200,000 metric tons

References

Andreae, M. O. and Gelencsér, A.: Black carbon or brown carbon? The nature of light-absorbing carbonaceous aerosols, Atmos. Chem. Phys., 6(3), 3419–3463, doi:10.5194/acpd-6-3419-2006, 2006.

Archibald, S., Nickless, A., Govender, N., RJ., S. and Lehsten, V.: Climate and the inter-annual variability of fire in southern Africa: a meta-analysis using long-term field data and satellite-derived burnt area data, Glob. Ecol. Biogeogr., 19(6), 794–809, 2010.

Baier, B. C., Brune, W. H., Lefer, B. L., Miller, D. O. and Martins, D. K.: Direct ozone production rate measurements and their use in assessing ozone source and receptor regions for Houston in 2013, Atmos. Environ., 114, 83–91, doi:10.1016/J.ATMOSENV.2015.05.033, 2015.

Baumgardner, D., Raga, G., Peralta, O., Rosas, I., Castro, T., Kuhlbusch, T., John, A. and Petzold, A.: Diagnosing black carbon trends in large urban areas using carbon monoxide measurements, J. Geophys. Res. Atmos., 107(21), doi:10.1029/2001JD000626, 2002.

Bond, T. C., Doherty, S. J., Fahey, D. W., Forster, P. M., Berntsen, T., DeAngelo, B. J., Flanner, M. G., Ghan, S., Kärcher, B., Koch, D., Kinne, S., Kondo, Y., Quinn, P. K., Sarofim, M. C., Schultz, M. G., Schulz, M., Venkataraman, C., Zhang, H., Zhang, S., Bellouin, N., Guttikunda, S. K., Hopke, P. K., Jacobson, M. Z., Kaiser, J. W., Klimont, Z., Lohmann, U., Schwarz, J. P., Shindell, D., Storelvmo, T., Warren, S. G. and Zender, C. S.: Bounding the role of black carbon in the climate system: A scientific assessment, J. Geophys. Res. Atmos., 118(11), 5380–5552, doi:10.1002/jgrd.50171, 2013.

Cai, H., Burnham, A. and Wang, M.: Updated Emission Factors of Air Pollutants from Vehicle Operations in GREET TM Using MOVES, , (September), 2013.

Carslaw, D. C. . and Ropkins, K.: The openair manual open-source tools for analysing air pollution data, King's Coll. London, 27–28(January), 287, 2012.

Chung, C. E., Kim, S. W., Lee, M., Yoon, S. C. and Lee, S.: Carbonaceous aerosol AAE inferred from in-situ aerosol measurements at the Gosan ABC super site, and the implications for brown carbon aerosol, Atmos. Chem. Phys., 12(14), 6173–6184, doi:10.5194/acp-12-6173-2012, 2012.

Crutzen, P. J. and Andreae, M.: Biomass Burning in the Tropics : Impact on Atmospheric Chemistry and Biogeochemical Cycles Estimates of Worldwide Biomass Burning, Science (80-.)., 250(4988), 1669–1678, doi:10.1126/science.250.4988.1669, 1990.

Dickerson, R. R., Andreae, M. O., Campos, T., Mayol-Bracero, O. L., Neususess, C. and Streets, D. G.: Analysis of black carbon and carbon monoxide observed over the Indian Ocean: Implications for emissions and photochemistry, J. Geophys. Res., 107(D19), doi:Artn 8017\rDoi 10.1029/2001jd000501, 2002.

Drinovec, L., Močnik, G., Zotter, P., Prévôt, A. S. H., Ruckstuhl, C., Coz, E., Rupakheti, M., Sciare, J., Müller, T., Wiedensohler, A. and Hansen, A. D. A.: The "dual-spot" Aethalometer: An improved measurement of aerosol black carbon with real-time loading compensation, Atmos. Meas. Tech., 8(5), 1965–1979, doi:10.5194/amt-8-1965-2015, 2015.

Dumka, U. C., Manchanda, R. K., Sinha, P. R., Sreenivasan, S., Moorthy, K. K. and Suresh Babu, S.: Temporal variability and radiative impact of black carbon aerosol over

680 tropical urban station Hyderabad, J. Atmos. Solar-Terrestrial Phys., 105–106(April
681 2016), 81–90, doi:10.1016/j.jastp.2013.08.003, 2013.
682 Field, R. D., van der Werf, G. R., Fanin, T., Fetzer, E. J., Fuller, R., Jethva, H., Levy, R.,
683 Livesey, N. J., Luo, M., Torres, O. and Worden, H. M.: Indonesian fire activity and smoke
684 pollution in 2015 show persistent nonlinear sensitivity to El Niño-induced drought,
685 Proc. Natl. Acad. Sci., 113(33), 9204–9209, doi:10.1073/pnas.1524888113, 2016.
686 Garg, S., Chandra, B. P., Sinha, V., Sarda-Esteve, R., Gros, V. and Sinha, B.: Limitation of
687 the Use of the Absorption Angstrom Exponent for Source Apportionment of
688 Equivalent Black Carbon: a Case Study from the North West Indo-Gangetic Plain,
689 Environ. Sci. Technol., 50(2), 814–824, doi:10.1021/acs.est.5b03868, 2016.
690 Gasore, J. and Physics, B. S.: Quantifying Emissions of Carbon Dioxide and Methane in
691 Central and Eastern Africa Through High Frequency Measurements and Inverse
692 Modeling, 2018.
693 Gatari, M. J. and Boman, J.: Black carbon and total carbon measurements at urban and
694 rural sites in Kenya, East Africa, Atmos. Environ., 37(8), 1149–1154,
695 doi:10.1016/S1352-2310(02)01001-4, 2003.
696 Geddes, J. A., Murphy, J. G. and Wang, D. K.: Long term changes in nitrogen oxides and
697 volatile organic compounds in Toronto and the challenges facing local ozone control,
698 Atmos. Environ., 43(21), 3407–3415, doi:10.1016/J.ATMOSENV.2009.03.053, 2009.
699 Gong, X., Kaulfus, A., Nair, U. and Jaffe, D. A.: Quantifying O3Impacts in Urban Areas
700 Due to Wildfires Using a Generalized Additive Model, Environ. Sci. Technol., 51(22),
701 13216–13223, doi:10.1021/acs.est.7b03130, 2017.
702 Harrison, R. M., Beddows, D. C. S., Hu, L. and Yin, J.: Comparison of methods for
703 evaluation of wood smoke and estimation of UK ambient concentrations, Atmos.
704 Chem. Phys., 12(17), 8271–8283, doi:10.5194/acp-12-8271-2012, 2012.
705 Hersey, S. P., Garland, R. M., Crosbie, E., Shingler, T., Sorooshian, A., Piketh, S. and
706 Burger, R.: An overview of regional and local characteristics of aerosols in South
707 Africa using satellite, ground, and modeling data, Atmos. Chem. Phys., 15(8), 4259–
708 4278, doi:10.5194/acp-15-4259-2015, 2015.
709 Horowitz, H. M., Garland, R. M., Thatcher, M., Landman, W. A., Dedekind, Z., Van Der
710 Merwe, J. and Engelbrecht, F. A.: Evaluation of climate model aerosol seasonal and
711 spatial variability over Africa using AERONET, Atmos. Chem. Phys., 17(22), 13999–
712 14023, doi:10.5194/acp-17-13999-2017, 2017.
713 Hsu, Y. K., Holsen, T. M. and Hopke, P. K.: Comparison of hybrid receptor models to
714 locate PCB sources in Chicago, Atmos. Environ., 37(4), 545–562, doi:10.1016/S1352-
715 2310(02)00886-5, 2003.
716 Kabashnikov, V. P., Chaikovsky, A. P., Kucsera, T. L. and Metelskaya, N. S.: Estimated
717 accuracy of three common trajectory statistical methods, Atmos. Environ., 45(31),
718 5425–5430, doi:10.1016/j.atmosenv.2011.07.006, 2011.
719 Kalnay, E., Kanamitsu, M., Kistler, R., Collins, W., Deaven, D., Gandin, L., Iredell, M.,
720 Saha, S., White, G., Woollen, J., Zhu, Y., Chelliah, M., Ebisuzaki, W., Higgins, W.,
721 Janowiak, J., Mo, K. C., Ropelewski, C., Wang, J., Leetmaa, A., Reynolds, R., Jenne, R. and
722 Joseph, D.: The NCEP/NCAR 40-year reanalysis project, Bull. Am. Meteorol. Soc., 77(3),
723 437–471, doi:10.1175/1520-0477(1996)077<0437:TNYRP>2.0.CO;2, 1996.
724 Kirchstetter, T. W. and Thatcher, T. L.: Contribution of organic carbon to wood smoke
725 particulate matter absorption of solar radiation, Atmos. Chem. Phys., 12(14), 6067–

726 6072, doi:10.5194/acp-12-6067-2012, 2012.
727 Koch, D., Schulz, M., Kinne, S., McNaughton, C., Spackman, J. R., Balkanski, Y., Bauer, S.,
728 Berntsen, T., Bond, T. C., Boucher, O., Chin, M., Clarke, A., De Luca, N., Dentener, F.,
729 Diehl, T., Dubovik, O., Easter, R., Fahey, D. W., Feichter, J., Fillmore, D., Freitag, S., Ghan,
730 S., Ginoux, P., Gong, S., Horowitz, L., Iversen, T., Kirkevåg, A., Klimont, Z., Kondo,
731 Y., Krol, M., Liu, X., Miller, R., Montanaro, V., Moteki, N., Myhre, G., Penner, J. E.,
732 Perlwitz, J., Pitari, G., Reddy, S., Sahu, L., Sakamoto, H., Schuster, G., Schwarz, J. P.,
733 Seland, Ø., Stier, P., Takegawa, N., Takemura, T., Textor, C., van Aardenne, J. a. and
734 Zhao, Y.: Evaluation of black carbon estimations in global aerosol models, Atmos.
735 Chem. Phys., 9(22), 9001–9026, doi:10.5194/acp-9-9001-2009, 2009.
736 Lack, D. A. and Langridge, J. M.: On the attribution of black and brown carbon light
737 absorption using the aerosol angstrom exponent, Atmos. Chem. Phys., 13(20), 10535–
738 10543, doi:10.5194/acp-13-10535-2013, 2013.
739 Lupu, A. and Maenhaut, W.: Application and comparison of two statistical trajectory
740 techniques for identification of source regions of atmospheric aerosol species, Atmos.
741 Environ., 36(36–37), 5607–5618, doi:10.1016/S1352-2310(02)00697-0, 2002.
742 Mkoma, S. L., Maenhaut, W., Chi, X., Wang, W. and Raes, N.: Characterisation of PM10
743 atmospheric aerosols for the wet season 2005 at two sites in East Africa, Atmos.
744 Environ., 43(3), 631–639, doi:10.1016/j.atmosenv.2008.10.008, 2009.
745 Monks, P. S., Archibald, A. T., Colette, A., Cooper, O., Coyle, M., Derwent, R., Fowler, D.,
746 Granier, C., Law, K. S., Mills, G. E., Stevenson, D. S., Tarasova, O., Thouret, V., Von
747 Schneidemesser, E., Sommariva, R., Wild, O. and Williams, M. L.: Tropospheric ozone
748 and its precursors from the urban to the global scale from air quality to short-lived
749 climate forcer, Atmos. Chem. Phys., 15(15), 8889–8973, doi:10.5194/acp-15-8889-
750 2015, 2015.
751 Moosmüller, H. and Chakrabarty, R. K.: Technical Note: Simple analytical relationships
752 between Ångström coefficients of aerosol extinction, scattering, absorption, and single
753 scattering albedo, Atmos. Chem. Phys., 11(20), 10677–10680, doi:10.5194/acp-11-
754 10677-2011, 2011.
755 Niang, I., Ruppel, O. C., Abdrabo, M. A., Essel, A., Lennard, C., Padgham, J. and Urquhart,
756 P.: Africa, Clim. Chang. 2014 Impacts, Adapt. Vulnerability - Contrib. Work. Gr. II to
757 Fifth Assess. Rep. Intergov. Panel Clim. Chang., 1199–1265,
758 doi:10.1017/CBO9781107415386.002, 2014.
759 Nyeki, S., Li, F., Weingartner, E., Streit, N., Colbeck, I., Gäggeler, H. W. and
760 Baltensperger, U.: The background aerosol size distribution in the free troposphere:
761 An analysis of the annual cycle at a high-alpine site, J. Geophys. Res. Atmos., 103(D24),
762 31749–31761, doi:10.1029/1998JD200029, 1998.
763 Otter, L. B., Scholes, R. J., Dowty, P., Privette, J., Caylor, K., Ringrose, S., Mukelabai, M.,
764 Frost, P., Hanan, N., Totolo, O. and Veenendaal, E. M.: The Southern African Regional
765 Science Initiative (SAFARI 2000): wet season campaigns, Situ, (April), 131–137,
766 2002.
767 Pan, X. L., Kanaya, Y., Wang, Z. F., Liu, Y., Pochanart, P., Akimoto, H., Sun, Y. L., Dong, H.
768 B., Li, J., Irie, H. and Takigawa, M.: Correlation of black carbon aerosol and carbon
769 monoxide in the high-altitude environment of Mt. Huang in Eastern China, Atmos.
770 Chem. Phys., 11(18), 9735–9747, doi:10.5194/acp-11-9735-2011, 2011.
771 Prinn, R. G., Weiss, R. F., Fraser, P. J., Simmonds, P. G., Cunnold, D. M., Alyea, F. N.,

772 O'Doherty, S., Salameh, P., Miller, B. R., Huang, J., Wang, R. H. J., Hartley, D. E., Harth, C.,
773 Steele, L. P., Sturrock, G., Midgley, P. M. and McCulloch, A.: A history of chemically and
774 radiatively important gases in air deduced from ALE/GAGE/AGAGE, J. Geophys. Res.
775 Atmos., 105(D14), 17751–17792, doi:10.1029/2000JD900141, 2000.
776 Ramanathan, V. and Carmichael, G.: Global and regional climate changes due to black
777 carbon, Nat. Geosci., 1, 221–227, doi:10.1038/ngeo156, 2008.
778 Real, E., Orlandi, E., Law, K. S., Fierli, F., Josset, D., Cairo, F., Schlager, H., Borrmann, S.,
779 Kunkel, D., Volk, C. M., McQuaid, J. B., Stewart, D. J., Lee, J., Lewis, A. C., Hopkins, J. R.,
780 Ravegnani, F., Ulanovski, A. and Liousse, C.: Cross-hemispheric transport of central
781 African biomass burning pollutants: Implications for downwind ozone production,
782 Atmos. Chem. Phys., 10(6), 3027–3046, doi:10.5194/acpd-9-17385-2009, 2010.
783 Russell, P. B., Bergstrom, R. W., Shinozuka, Y., Clarke, a. D., DeCarlo, P. F., Jimenez, J. L.,
784 Livingston, J. M., Redemann, J., Holben, B., Dubovik, O. and Strawa, A.: Absorption
785 Angstrom Exponent in AERONET and related data as an indicator of aerosol
786 composition, Atmos. Chem. Phys., 10, 1156–1169, doi:10.5194/acpd-9-21785-2009,
787 2010.
788 Saarikoski, S., Carbone, S., Decesari, S., Giulianelli, L., Angelini, F., Canagaratna, M., Ng,
789 N. L., Trimborn, a., Facchini, M. C., Fuzzi, S., Hillamo, R. and Worsnop, D.: Chemical
790 characterization of springtime submicrometer aerosol in Po Valley, Italy, Atmos.
791 Chem. Phys., 12(18), 8401–8421, doi:10.5194/acp-12-8401-2012, 2012.
792 Safari, B. K. (University of R. and Gasore, J. (University of R.: Estimation of Global Solar
793 Radiation in Rwanda Using Empirical Models, Asian J. Sci. Res., 2(2), 68–75,
794 doi:10.3923/ajsr.2009.68.75, 2009.
795 Sahu, L. K., Kondo, Y., Moteki, N., Takegawa, N., Zhao, Y., Cubison, M. J., Jimenez, J. L.,
796 Vay, S., Diskin, G. S., Wisthaler, A., Mikoviny, T., Huey, L. G., Weinheimer, A. J. and
797 Knapp, D. J.: Emission characteristics of black carbon in anthropogenic and biomass
798 burning plumes over California during ARCTAS-CARB 2008, J. Geophys. Res. Atmos.,
799 117(16), 1–20, doi:10.1029/2011JD017401, 2012.
800 Saleh, R., Hennigan, C. J., McMeeking, G. R., Chuang, W. K., Robinson, E. S., Coe, H.,
801 Donahue, N. M. and Robinson, A. L.: Absorptivity of brown carbon in fresh and photo-
802 chemically aged biomass-burning emissions, Atmos. Chem. Phys., 13(15), 7683–7693,
803 doi:10.5194/acp-13-7683-2013, 2013.
804 Saleh, R., Robinson, E. S., Tkacik, D. S., Ahern, A. T., Liu, S., Aiken, A. C., Sullivan, R. C.,
805 Presto, A. a., Dubey, M. K., Yokelson, R. J., Donahue, N. M. and Robinson, A. L.:
806 Brownness of organics in aerosols from biomass burning linked to their black carbon
807 content, Nat. Geosci., 7(September), 1–4, doi:10.1038/ngeo2220, 2014.
808 Sandradewi, J., Prévôt, A. S. H., Szidat, S., Perron, N., Alfarra, M. R., Lanz, V. A.,
809 Weingartner, E. and Baltensperger, U.: Using Aerosol Light Absorption Measurements
810 for the Quantitative Determination of Wood Burning and Traffic Emission
811 Contributions to Particulate Matter, Environ. Sci. Technol., 42(9), 3316–3323,
812 doi:10.1021/es702253m, 2008.
813 Sauvage, B., Thouret, V., Cammas, J. P., Gheusi, F., Athier, G. and Nédélec, P.:
814 Tropospheric ozone over Equatorial Africa: regional aspects from the MOZAIC data,
815 Atmos. Chem. Phys., 5, 311–335, doi:10.5194/acpd-4-3285-2004, 2005.
816 Seibert, P., Kromp-Kolb, H., Baltensperger, U., Jost, D. T. and Schwikowski, M.:
817 Trajectory Analysis of High-Alpine Air Pollution Data, in Air Pollution Modeling and

Its Application: NATO: Challenges of Modern Society, edited by S.-E. (Riso N. L. Gryning and M. M. (Centre for E. S. of the M. Millan, pp. 595–596, Springer USA., 1994.
Tesfaye, M., Sivakumar, V., Botai, O. and Mengistu Tsidu, G.: Aerosol climatology over South Africa based on 10 years of Multiangle Imaging Spectroradiometer (MISR) data., 2011.
Thompson, A. M., Diab, R. D., Bodeker, G. E., Zunckel, M., Coetzee, G. J. R., Archer, C. B., Mcnamara, D. P., Pickering, K. E., Combrink, J., Fishman, J. and Nganga, D.: Ozone over southern Africa during SAFARI-92 / TRACE A, , 101(95), 1996.
van Vliet, E. D. S. and Kinney, P. L.: Impacts of roadway emissions on urban particulate matter concentrations in sub-Saharan Africa: new evidence from Nairobi, Kenya, Environ. Res. Lett., 2(4), 045028, doi:10.1088/1748-9326/2/4/045028, 2007.
Welp, L. R., Keeling, R. F., Weiss, R. F., Paplawsky, W. and Heckman, S.: Design and performance of a Nafion dryer for continuous operation at CO2and CH4 air monitoring sites, Atmos. Meas. Tech., 6(5), 1217–1226, doi:10.5194/amt-6-1217-2013, 2013.
WHO: Health Effects of Particulate Matter: Policy imlications for countries in eastern Europe, Caucasus and central Asia, World Heal. Organ., 15 [online] Available from: www.euro.who.int, 2013.
World Health Organization: Ambient air pollution: A global assessment of exposure and burden of diseas, World Heal. Organ., doi:9789241511353, 2016.
Yuan, J. F., Huang, X. F., Cao, L. M., Cui, J., Zhu, Q., Huang, C. N., Lan, Z. J. and He, L. Y.: Light absorption of brown carbon aerosol in the PRD region of China, Atmos. Chem. Phys., 16(3), 1433–1443, doi:10.5194/acp-16-1433-2016, 2016.
Zhang, L., Jin, L., Zhao, T., Yin, Y., Zhu, B., Shan, Y., Guo, X., Tan, C., Gao, J. and Wang, H.: Diurnal variation of surface ozone in mountainous areas: Case study of Mt. Huang, East China, Sci. Total Environ., 538, 583–590, doi:10.1016/j.scitotenv.2015.08.096, 2015.

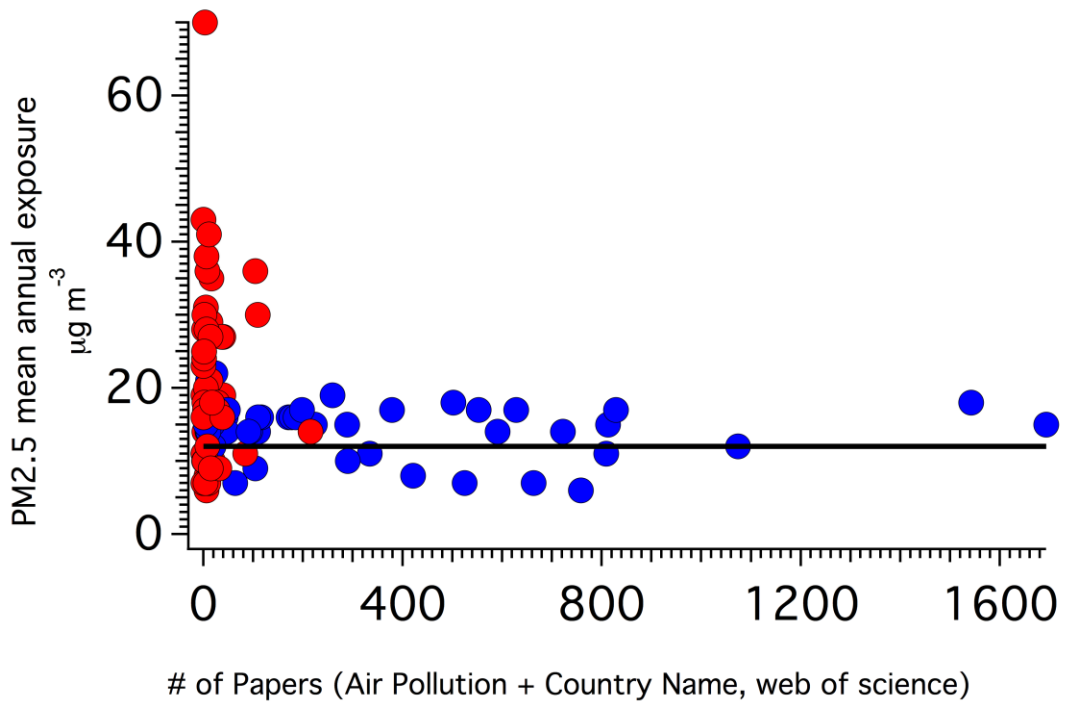

Figure 1: Africa (red) and Europe (blue), $PM_{2.5}$ mean annual exposure (https://data.worldbank.org/indicator/en.atm.pm25.mc.m3) and paper count of country + air pollution (from Web of Science).

Figure 2. From top left moving counter-clockwise: an aerial view of RCO at Mt. Mugogo Main Peak, the station with towers in the background, and the location of Mt. Mugogo in Rwanda (blue pin) in relation to Kigali (yellow pin).

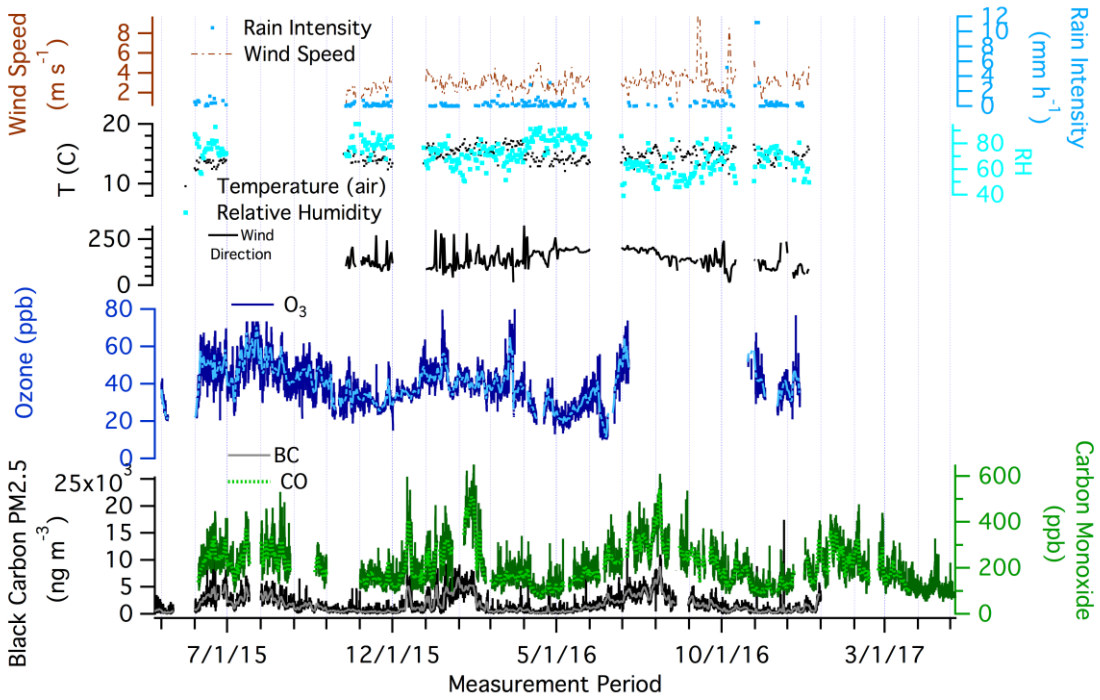

869

870

871 **Figure 3**. From the top down up: (a) wind speed (red dotted) and rain intensity (blue

872 dash) daily average values; (b) temperature (black) and relative humidity (light blue)

873 values; (c) ozone (dark blue, light blue) (15 minute, daily); (d) black carbon (black,

874 grey) and carbon monoxide (dark green, light green) (15 minute, daily) average

875 concentrations.

876

877
878
879
880
881
882
883
884
885
886
887

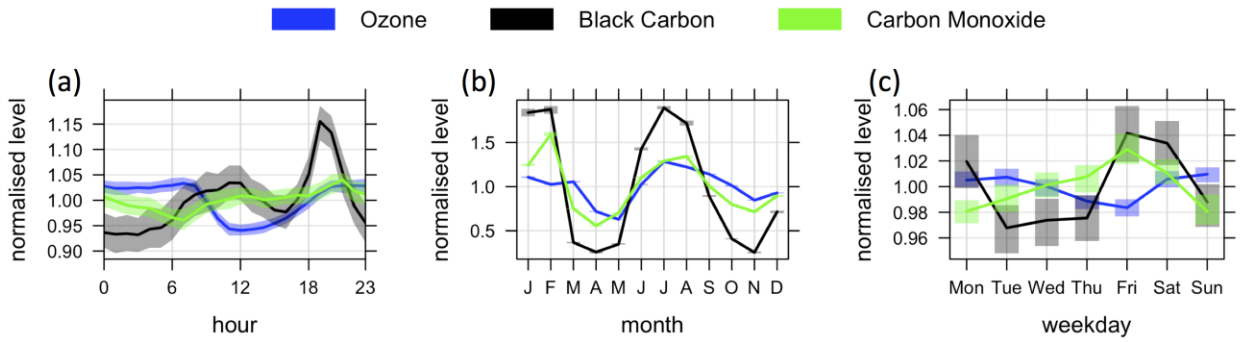

Figure 4. Normalized temporal variations of O_3 mixing ratios, CO mixing ratios, and BC concentrations by: (a) hour (diurnal) (b) month, and (c) day of the week. Shaded areas are 95% confidence intervals.

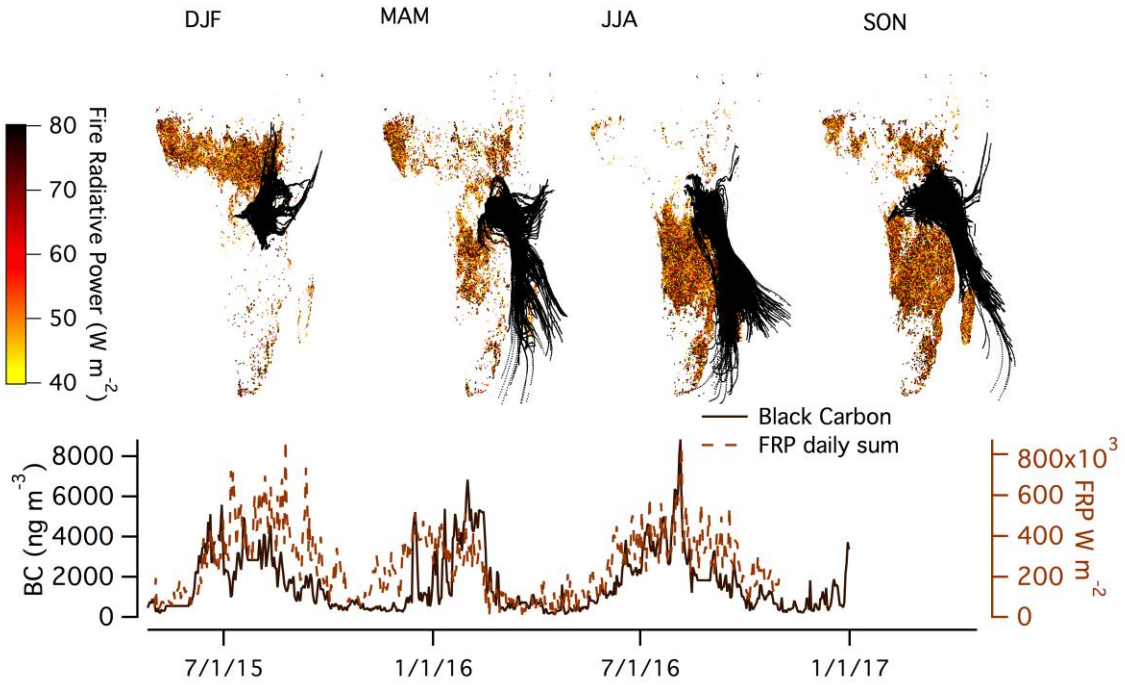

Figure 5. (a) Seasonal fire radiative power data acquired with the MODIS instrument and back trajectories of air masses (generated with the HYSPLIT model) reaching the Rwanda Climate Observatory for the period May 2015 to January 2017. Seasons in Rwanda are split into: short dry season, December-January-February (DJF), long rainy season, March-April-May (MAM), long dry season, June-July-August (JJA,) and short rainy season, September-October-November (SON). (b) The time series of daily average BC concentration and the daily sum of Fire Radiative Power (W m^{-2}) from the pictured data bound by the furthest HYSPLIT backtrajectory reaches each season (box defined by the most north, south, east, and west point the HYSPLIT backtrajectories reach).

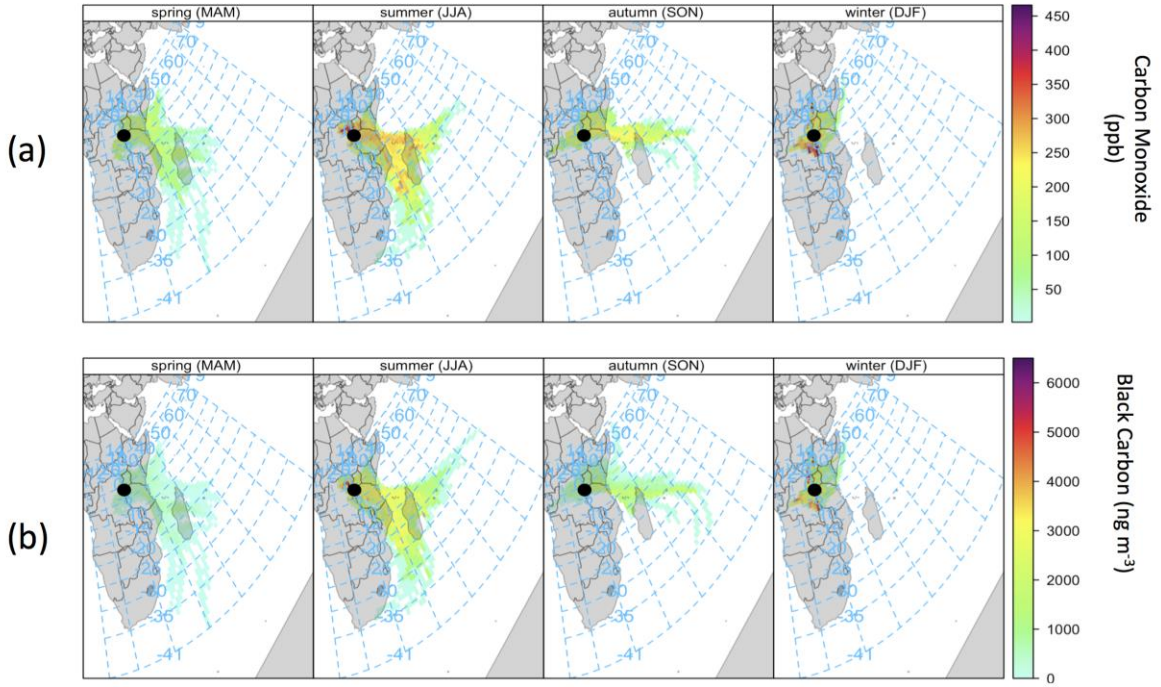

Figure 6. Concentration-weighted back trajectories of (a) CO and (b) BC, separated by season, for measurements at the Rwanda Climate Observatory (black dot) for the period of July 2015-January 2017.

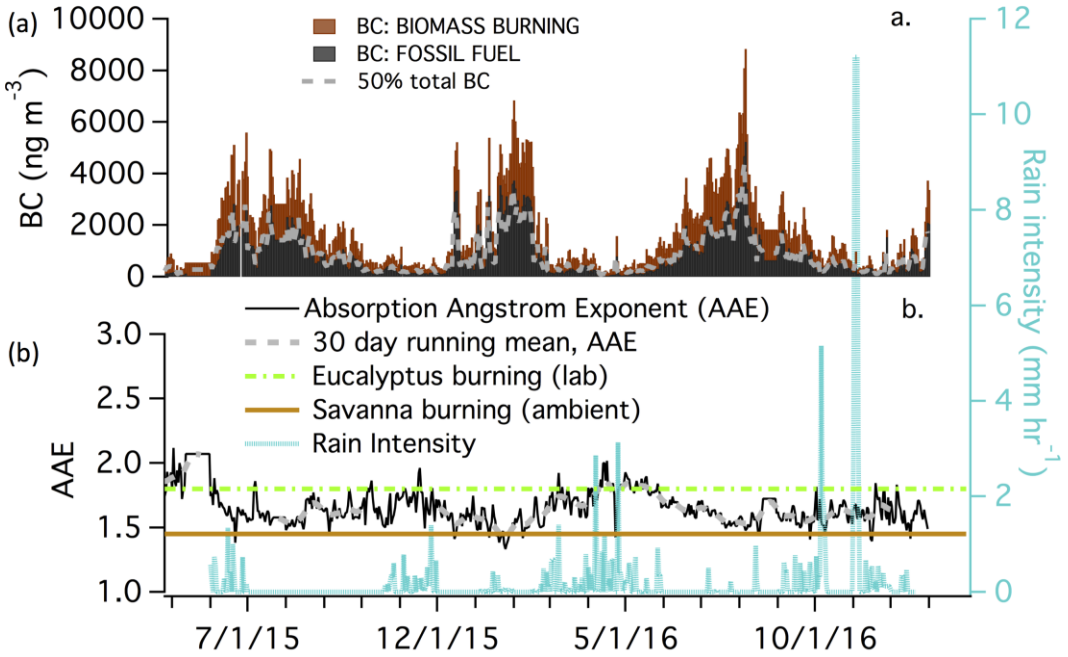

Figure 7. (a) Time series of contributions of fossil fuel combustion and biomass burning to BC concentrations observed at RCO. (b) Daily average absorption Angstrom exponent (AAE) measured at RCO (black line), rain intensity, and published AAE for Eucalyptus burning ((Yuan et al., 2016), laboratory studies, green line) and savanna burning ((Russell et al., 2010), ambient, brown line) also shown as reference.

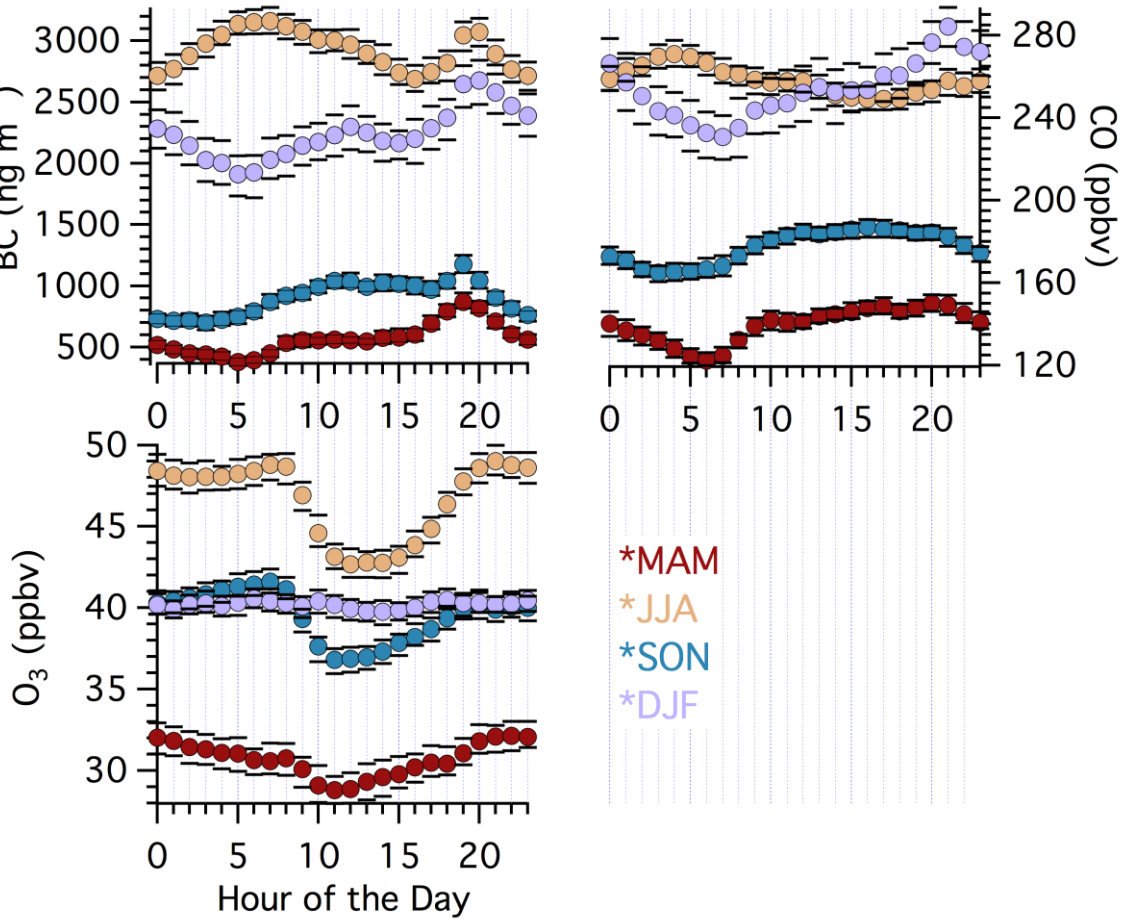

Figure 8. Seasonally separated diurnal profiles of (a) BC concentrations, (b) CO mixing ratios, and (c) O_3 mixing ratios, colored for each season. The circles represent mean concentrations and the lines represent 95% confidence intervals.

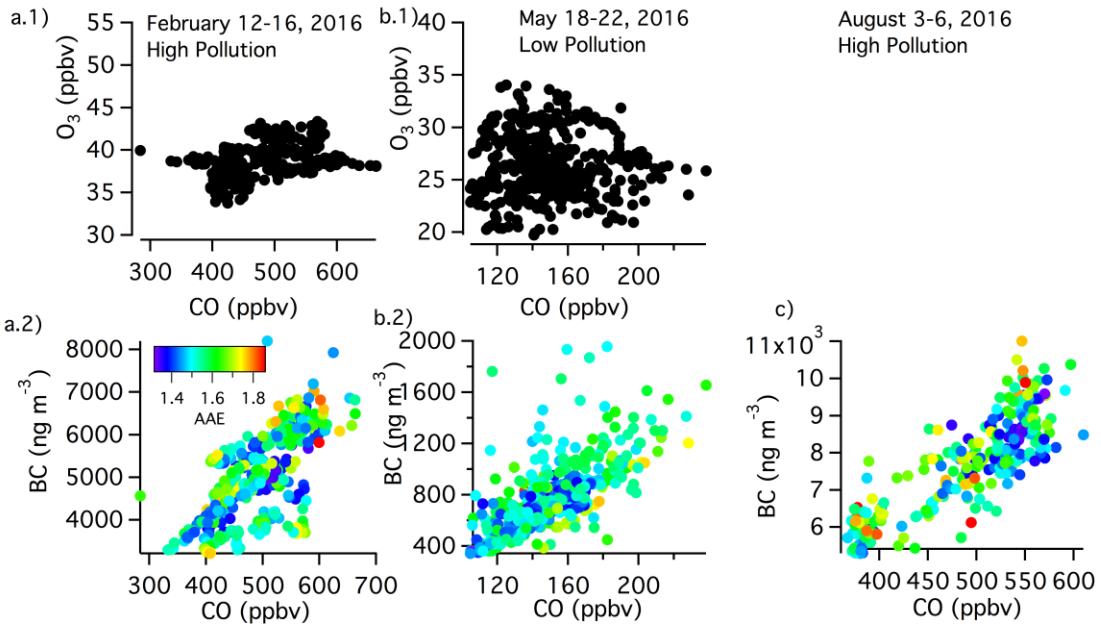

Figure 9: Polluted period in DJF (a), non-polluted period in MAM (b), and polluted period in JJA (c). Comparison of O3 and CO in a.1 and b.1, and comparison of BC and CO, color-coded by AAE, in a.2, b.2, and c for each respective period.

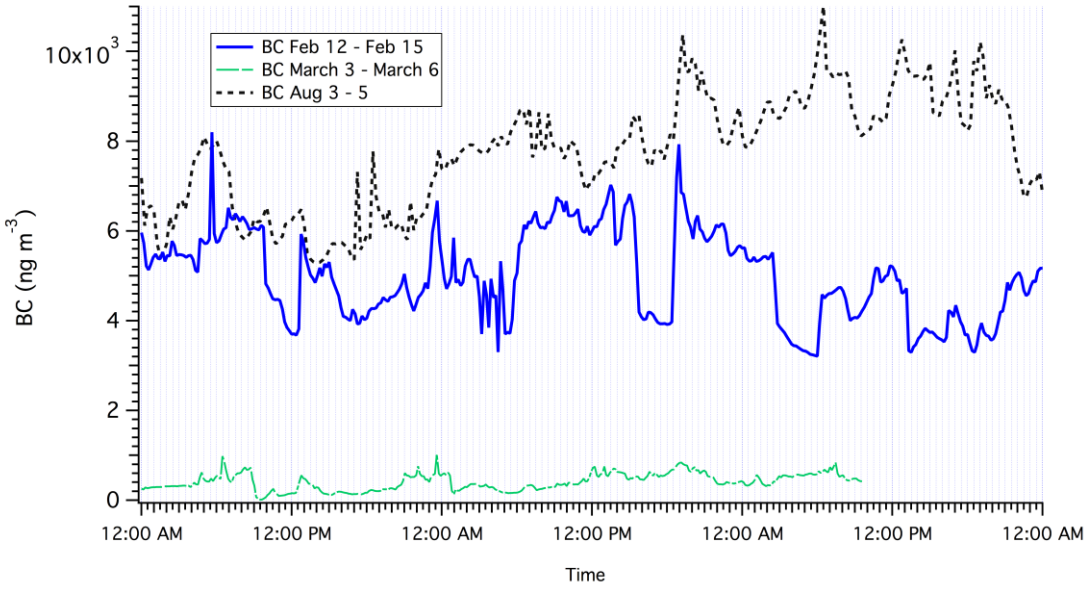

Figure 10: Case study of BC in a polluted period in February (blue line), a non-polluted period in March (green line), and a polluted period in August (dotted black line).

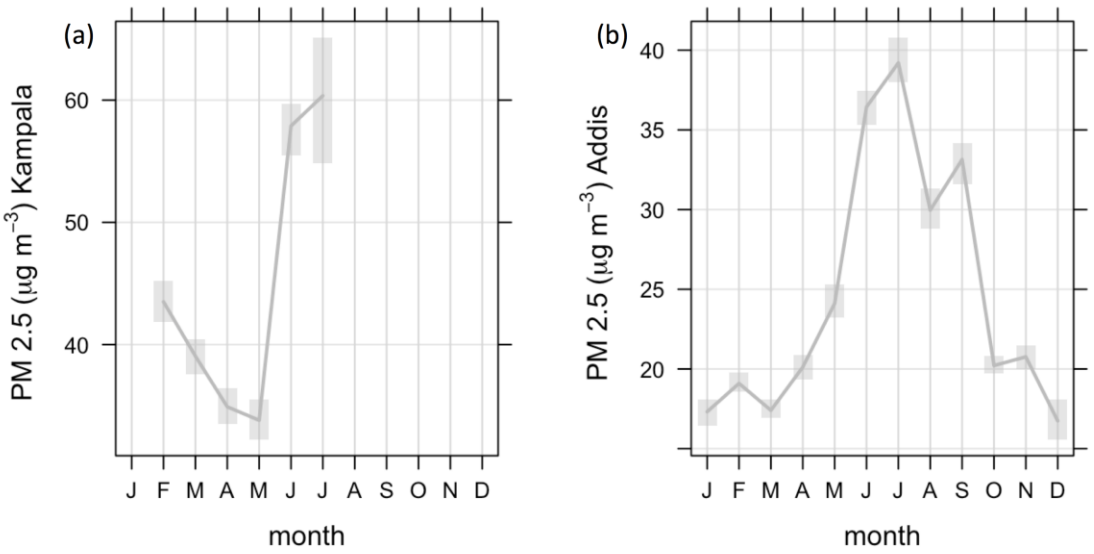

Figure 11: Monthly means of $PM_{2.5}$ concentrations measured at the US Embassies in (**a**) Kampala, Uganda (as available) and (**b**) Addis Ababa, Ethiopia (right) from January-December 2016/2017 (as available). Shaded areas are 95% confidence intervals. Lines indicate daily average WHO recommendation for healthy $PM_{2.5}$ limits.